

# Simulations of cubic-tetragonal ferroelastics

A. E. Jacobs<sup>1\*</sup>, S. H. Curnoe<sup>2†</sup> and R. C. Desai<sup>1‡</sup>

<sup>1</sup>*Department of Physics, University of Toronto, Toronto, Ont., M5S 1A7, Canada*

<sup>2</sup>*Department of Physics and Physical Oceanography, Memorial University of Newfoundland, St. John's, Nfld. & Lbdr., A1B 3X7, Canada*

(October 31, 2018)

We study domain patterns in cubic-tetragonal ferroelastics by solving numerically equations of motion derived from a Landau model of the phase transition, including dissipative stresses. Our system sizes, of up to  $256^3$  points, are large enough to reveal many structures observed experimentally. Most patterns found at late stages in the relaxation are multiply banded; all three tetragonal variants appear, but inequivalently. Two of the variants form broad primary bands; the third intrudes into the others to form narrow secondary bands with the hosts. On colliding with walls between the primary variants, the third either terminates or forms a chevron. The multiply banded patterns, with the two domain sizes, the chevrons and the terminations, are seen in the microscopy of zirconia and other cubic-tetragonal ferroelastics. We examine also transient structures obtained much earlier in the relaxation; these show the above features and others also observed in experiment.

PACS numbers: 81.30.Kf, 62.20.Dc

## I. INTRODUCTION

Ferroelastics<sup>1–3</sup> are crystalline solids that undergo a shape-changing, structural phase transition with decreasing temperature  $T$ . The high- $T$  or *parent* phase distorts spontaneously at the transition temperature  $T_c$  to form one or more *products* or *variants* with identical energies but different orientations. In cubic-tetragonal (C-T) ferroelastics for example, only one of three four-fold axes is retained below  $T_c$ , giving three variants.

Due to constraints imposed by neighbouring material, a single variant is found only rarely, perhaps only in very small grains; the displacement resulting from a strain of  $10^{-4}$  in a grain of size  $10\ \mu\text{m}$  (both typical values) is an order of magnitude too large to be accommodated by atomic rearrangements at grain boundaries. Multiple variants can arise also from independent nucleation events. An external stress can move the walls that separate the variants, so converting one variant to the other(s) at little cost in energy; the process has been observed for example by neutron diffraction of zirconia<sup>4</sup>. Related phenomena are strongly hysteretic stress-strain relations, shape-memory effects, etc<sup>3</sup>.

Pockets of the parent phase can persist below  $T_c$ , until the gain in condensation energy overcomes the cost of introducing domain walls. Compositional inhomogeneities combined with a strong dependence of  $T_c$  on composition can also smear the transition, in cases to over 100 K; it is common to speak instead of a transformation.

Domain patterns in ferroelastics have nothing in common with those in conventional order-parameter systems. Two-dimensional (2d) patterns in tetragonal-orthorhombic (T-O) ferroelastics like  $\text{YBa}_2\text{Cu}_3\text{O}_{7-\delta}$  resemble not at all those in 2d Ising models, though both have two variants; neither can 2d patterns in hexagonal-orthorhombic (H-O) ferroelastics be understood from 2d three-state Potts models, both with three. The difference arises because (a) in order to maintain a coherent

interface (no dislocations or disclinations), ferroelastic domain walls rotate the variants as well as join them, and (b) order-parameter strains alone are insufficient to understand the patterns. Disclinations, which have no counterpart in Ising and Potts systems, are generated however by wall collisions; they dominate patterns especially in H-O-like systems (e.g. trigonal-monoclinic lead orthovanadate).

Much of ferroelastic theory follows Barsch and Krumhansl<sup>5</sup> in expanding the free-energy density in powers of the strains and their derivatives. Analytical results are possible in a few cases<sup>5,6</sup>, but structures formed by colliding walls require numerical effort for their understanding. Such studies<sup>7–9</sup> in 2d gave static and transient domain patterns that reproduced nearly all aspects of those observed in H-O-like and T-O ferroelastics. Ref. 10 obtained similar results.

An alternative approach, phase-field theory<sup>11</sup>, predates Ref. 5 and has also been used extensively to understand domain patterns in H-O-like materials<sup>12</sup>, C-T materials<sup>13,14</sup>, etc. Ref. 15 discusses differences between the two approaches. And other lines have been pursued.

In C-T ferroelastics, domain walls joining two tetragonal variants lie optimally in the cubic 110 planes<sup>16</sup> and are then twin walls. In the solutions<sup>5,17,18</sup> for the twin wall, the strains depart only locally from their bulk values, decaying exponentially with distance from the wall. Of course domain walls need not lie in the cubic 110 planes; they are then not twin walls, and the departures decay algebraically<sup>19</sup>.

Optical and electron microscopy of zirconia<sup>20–22</sup>, leucite<sup>23,3</sup>, barium titanate<sup>2</sup> and other<sup>24</sup> C-T ferroelastics reveals a variety of patterns. The structures<sup>2</sup> of small and large grains are respectively lamellar (with only two variants) and banded (with all three); the latter seems unique to C-T materials. The lamellar  $\leftrightarrow$  banded transition is understood<sup>2,25</sup>, though the analysis is apparently limited to variants oriented at  $\pi/2$ . Other as-

pects of the domain patterns have also been explained analytically<sup>20,26,2,25</sup>. The character of the patterns depends also on the thickness of the sample and on whether the surface examined is part of clamped specimen, or a free surface, or representative of the bulk<sup>2,25</sup>. The highly sensitive technique of birefringence imaging<sup>27</sup> promises to reveal further details of these patterns.

The following presents results from simulating the time evolution of C-T materials. We obtain the equations of motion by expanding the free-energy density and the Rayleigh dissipation density to lowest possible order in the strains and their derivatives. We solve numerically for the displacement, using periodic boundary conditions and omitting the inertial term. Our late-time structures reproduce most features of the banded patterns found in C-T materials<sup>2,3,20-24</sup>. These structures were not found in the smaller systems used in the previous C-T simulations of Refs. 28 and 29; some were found in a phase-field study<sup>14</sup>. Our transient structures show in addition other wall configurations observed experimentally.

## II. LANDAU THEORY AND EQUATIONS OF MOTION OF ELASTICS

The displacement  $\mathbf{u}(\mathbf{r})$  of a material point is defined relative to its position  $\mathbf{r}$  in the parent phase. The symmetric strain tensor in this Lagrangian description is  $\eta_{ij} = \frac{1}{2}(u_{i,j} + u_{j,i} + u_{k,i}u_{k,j})$ , where  $u_{i,j} = \partial u_i / \partial x_j$ . We neglect the nonlinear term in  $\eta$  because it has no known qualitative effect on the domain patterns. The strains (all of which vanish in the parent phase) are defined by

$$e_1 = u_{1,1} + u_{2,2} + u_{3,3} , \quad (1)$$

$$e_2 = \frac{1}{2}(u_{1,1} - u_{2,2}) , \quad (2)$$

$$e_3 = \frac{1}{2\sqrt{3}}(u_{1,1} + u_{2,2} - 2u_{3,3}) , \quad (3)$$

$$e_4 = \frac{1}{2}(u_{2,3} + u_{3,2}) , \quad (4)$$

$$e_5 = \frac{1}{2}(u_{3,1} + u_{1,3}) , \quad (5)$$

$$e_6 = \frac{1}{2}(u_{1,2} + u_{2,1}) ; \quad (6)$$

these definitions differ slightly from those in Ref. 18. The deviatoric strains  $e_2$  and  $e_3$  form the two-component order parameter of the transition. The other strains  $e_1$  (the dilatational strain in the small-strain limit) and the shear strains  $e_4$ ,  $e_5$  and  $e_6$  are identically zero in the uniform product phase; they are required however to understand domain patterns, even for a single twin wall<sup>5,17,18</sup>.

The six strains are obtained from the three components of the displacement  $\mathbf{u}$  and so are not independent when they vary spatially; the second derivatives of the strains are linked by *compatibility relations*, necessary and sufficient conditions that the strains be derivable from  $\mathbf{u}$ . We satisfy these relations implicitly by working with the components  $u_i$ . Refs. 30, 29, 10, which work directly with the strains, satisfy them explicitly by imposing them to obtain nonlocal relations between the order-parameter

strains  $e_2$  and  $e_3$ ; the anisotropic, oscillatory nature of the kernels, obtained also in Ref. 15, provides much insight into domain structures and their relaxation. Nonlocal relations were developed much earlier<sup>11</sup>, though there appear to be differences<sup>15</sup>.

In the Landau expansion of the free-energy density in the strains and their derivatives, the cubic symmetry of the parent phase permits three invariants to second order in the strains,  $e_1^2$ ,  $e_2^2 + e_3^2$  and  $e_4^2 + e_5^2 + e_6^2$ . The corresponding stiffness coefficients  $A_1$ ,  $A_2$  and  $A_4$  are linear combinations of the Voigt coefficients. The order-parameter stiffness  $A_2$  softens with decreasing  $T$  as  $A_2 = \alpha(T - T_0)$ . To describe the phase transition, one adds a term cubic in  $e_2$  and  $e_3$  (this term breaks the rotational symmetry in  $(e_2, e_3)$  space), and a quartic term for stability. The minimal density, that contains only essential terms, is

$$\begin{aligned} \mathcal{F} = & \frac{A_1}{2} e_1^2 + \frac{A_2}{2} (e_2^2 + e_3^2) - \frac{B_2}{3} (e_3^3 - 3e_2^2 e_3) \\ & + \frac{C_2}{4} (e_2^2 + e_3^2)^2 + \frac{A_4}{2} (e_4^2 + e_5^2 + e_6^2) \\ & + \frac{D_2}{2} [(\nabla e_2)^2 + (\nabla e_3)^2] ; \end{aligned} \quad (7)$$

the last term gives the domain-wall energy (which prevents the system from dividing into arbitrarily small domains). We omit all unnecessary terms, namely higher-order terms and also some of the same order as those kept (a second invariant in the order-parameter derivatives<sup>18,29</sup> and other derivative invariants).

The coefficients  $A_2$ ,  $B_2$  and  $C_2$  determine the transition temperature  $T_c$  and the spontaneous strain  $e_{30}$  in the product phase. When  $A_2 > B_2^2/4C_2$ , the free energy has only the cubic minimum at  $e_2 = e_3 = 0$ . For  $A_2 < B_2^2/4C_2$ , it has also three degenerate tetragonal minima located at

$$e_2 = 0 , \quad e_3 = e_{30} \quad (8)$$

$$e_2 = -\sqrt{3}e_{30}/2 , \quad e_3 = -e_{30}/2 \quad (9)$$

$$e_2 = \sqrt{3}e_{30}/2 , \quad e_3 = -e_{30}/2 \quad (10)$$

with (we assume  $B_2 > 0$ )

$$e_{30} = \frac{B_2 + (B_2^2 - 4A_2C_2)^{1/2}}{2C_2}. \quad (11)$$

The phase transition, which is first-order, occurs when  $A_2 = \frac{2}{9}B_2^2/C_2$ . The cubic phase is unstable for  $A_2 < 0$ .

The symmetric stress tensor  $\sigma_{ij}$  is defined by

$$\sigma_{ij} = \delta\mathcal{F}/\delta\eta_{ij} = \mathcal{G}_k \delta e_k / \delta\eta_{ij} \quad (12)$$

with  $\mathcal{G}_k \equiv \delta\mathcal{F}/\delta e_k$ ; explicitly,

$$\mathcal{G}_2 = (A_2 - D_2\nabla^2) e_2 + 2B_2 e_2 e_3 + C_2 e_2 (e_2^2 + e_3^2) \quad (13)$$

$$\mathcal{G}_3 = (A_2 - D_2\nabla^2) e_3 + B_2 (e_2^2 - e_3^2) + C_2 e_3 (e_2^2 + e_3^2) \quad (14)$$

$$\sigma_{11} = A_1 e_1 + \frac{1}{2} \mathcal{G}_2 + \frac{1}{2\sqrt{3}} \mathcal{G}_3 \quad (15)$$

$$\sigma_{22} = A_1 e_1 - \frac{1}{2} \mathcal{G}_2 + \frac{1}{2\sqrt{3}} \mathcal{G}_3 \quad (16)$$

$$\sigma_{33} = A_1 e_1 - \frac{1}{\sqrt{3}} \mathcal{G}_3 \quad (17)$$

$$\sigma_{23} = A_4 e_4 \quad (18)$$

$$\sigma_{31} = A_4 e_5 \quad (19)$$

$$\sigma_{12} = A_4 e_6 \quad (20)$$

Stresses arise also from dissipative mechanisms. The same symmetry considerations as used for the free energy give the Rayleigh dissipative density as

$$\mathcal{R} = \frac{A'_1}{2} \dot{e}_1^2 + \frac{A'_2}{2} (\dot{e}_2^2 + \dot{e}_3^2) + \frac{A'_4}{2} (\dot{e}_4^2 + \dot{e}_5^2 + \dot{e}_6^2) \quad (21)$$

to lowest order in the time derivatives  $\dot{e}_j$  of the strains. The dissipative stresses  $\sigma'_{ij}$  are found from

$$\sigma'_{ij} = \delta \mathcal{R} / \delta \dot{\eta}_{ij} = \mathcal{G}'_k \delta \dot{e}_k / \delta \dot{\eta}_{ij} \quad (22)$$

where  $\mathcal{G}'_k \equiv \delta \mathcal{R} / \delta \dot{e}_k$ :  $\mathcal{G}'_1 = A'_1 \dot{e}_1, \dots, \mathcal{G}'_6 = A'_4 \dot{e}_6$ .

Our interest is in static states and in states where walls move slowly (rather than in effects associated with motion at or near the sound velocity) and so we assume isothermal conditions. The equations of motion follow from Newton's second law

$$f_i = \rho \ddot{u}_i = \sigma'_{ij,j} + \sigma_{ij,j} . \quad (23)$$

In the overdamped limit, the inertial term  $\rho \ddot{u}_i$  is dropped and Eq.(23) simplifies to  $\sigma'_{ij,j} = -\sigma_{ij,j}$ . In terms of the displacement, this is

$$\begin{aligned} & [A' \partial_1^2 + B' (\partial_2^2 + \partial_3^2)] \dot{u}_1 + C' (\partial_1 \partial_2 \dot{u}_2 + \partial_1 \partial_3 \dot{u}_3) \\ &= - (A - \frac{1}{3} D_2 \nabla^2) \partial_1^2 u_1 - B (\partial_2^2 + \partial_3^2) u_1 \\ & - (C + \frac{1}{6} D_2 \nabla^2) (\partial_1 \partial_2 u_2 + \partial_1 \partial_3 u_3) + R_1^{NL} \end{aligned} \quad (24)$$

for  $i = 1$ , with obvious forms for  $i = 2, 3$ . The coefficients are  $A' = A'_1 + \frac{1}{3} A'_2$ ,  $B' = \frac{1}{4} A'_4$  and  $C' = A'_1 - \frac{1}{6} A'_2 + \frac{1}{4} A'_4$ ; the definitions for  $A$ ,  $B$  and  $C$  are obtained by dropping the primes. The nonlinear terms

$$R_1^{NL} = -\partial_1 \left( \frac{1}{2} \mathcal{G}_2^{NL} + \frac{1}{2\sqrt{3}} \mathcal{G}_3^{NL} \right) \quad (25)$$

$$R_2^{NL} = -\partial_2 \left( -\frac{1}{2} \mathcal{G}_2^{NL} + \frac{1}{2\sqrt{3}} \mathcal{G}_3^{NL} \right) \quad (26)$$

$$R_3^{NL} = -\partial_3 \left( -\frac{1}{\sqrt{3}} \mathcal{G}_3^{NL} \right) \quad (27)$$

on the right-hand sides involve the nonlinear parts of  $\mathcal{G}_2$  and  $\mathcal{G}_3$ , namely the terms with coefficients  $B_2$  and  $C_2$  in Eqs.(13) and (14).

The matrix on the left-hand side of Eq.(24) must be invertible. Special handling is required when the strains are constant (that is  $\partial_1 = \partial_2 = \partial_3 = 0$ ) since both sides are then zero. Examining the full equation of motion

(23), we see that the proper way to account for the constant strains is to leave them constant at all times. The interpretation is physical: a piece of strained material does not move unless there is a differential strain. Another case of interest is  $A'_1 = A'_4 = 0$ , which may be a reasonable choice given that it is the order parameter, and not the other strain components, which changes most quickly in time. Then the matrix is not invertible for  $\partial_1 = 0$  or  $\partial_2 = 0$  or  $\partial_3 = 0$ , but again Eq.(23) tells us how to handle this case.

The equations of motion (24) can be solved under a variety of boundary conditions. Wishing to examine domain patterns, we used periodic boundary conditions (which allow no length change in any direction) in order to force domain walls into the low- $T$  phase; all three variants are required since two variants can satisfy the constraint in only two directions. A second important consideration is that these conditions allow use of the fast Fourier transform, which is much faster than real-space methods. We should however voice our concern that these conditions may lead to spurious correlations between relaxation events at large relative distances. Of other choices, clamped conditions ( $\mathbf{u} = 0$  on and outside the boundaries, as in Ref. 8) would also force domain walls into the low- $T$  phase, but are less attractive because they usually give complex structures near the edges. Open conditions are not useful for our purpose, for the system would go to a single variant for almost any initial state. Yet another possibility corresponds to applied stresses at the boundaries.

In Fourier space, Eqs. (24) are identical to the equations of time-dependent Ginzburg-Landau (TDGL) theory<sup>30,29,10</sup>. In real space, Eqs. (24) contain extra space derivatives on both sides relative to TDGL theory and so appear more general (they can be applied for example to systems with imposed strains). The neglect of the inertial terms both here and in Refs. 30, 29, 10 is problematic for the relaxation.

### III. DOMAIN PATTERNS

We solved Eqs.(24) numerically, as described in the Appendix, starting usually from random displacements. We present fully converged<sup>31</sup> results for 3d grids of  $128^3$  points and quasi-static<sup>31</sup> results for  $256^3$  points. We present also transient structures in systems of  $256^3$  points. Systems of these sizes reveal features not seen in previous studies, which used at most  $64^3$  points.

The nature of the patterns depends in part on the stiffness coefficients  $A_1$  and  $A_4$ . The dilatational and shear energies are minimized when the walls lie in cubic 110 planes, and so the parameters  $A_1$  and  $A_4$  control the energy cost incurred when the walls depart from their optimal orientations. In stiff systems, with large  $A_1$  and  $A_4$ , the domain walls must lie close to the 110 planes, whereas in soft systems they can depart from these opti-

mal orientations at small cost in energy. We have however no quantitative way to distinguish stiff from soft systems; comparing  $A_1$  and  $A_4$  with the order-parameter stiffnesses<sup>7</sup> found from the curvatures of the free energy about the tetragonal minima is not an effective means.

### A. Late-time structures

We made extensive studies of late-time domain structures at  $A_2 = -2$  and  $A_2 = -20$ ; the spontaneous strain  $e_{30}$  at these temperatures is respectively twice and four times the value at  $T_c$ . We present results at only the lower (latter) value, where the order parameters inside the domains are more well developed.

Most of  $\approx 200$  simulations gave multiply banded or herringbone structures like those shown in Figure 1<sup>32</sup>. These patterns, which seem at first glance to reflect more the periodic boundary conditions than any physics, are in fact found in the microstructure of polydomain zirconia (examples are Figures 4(a), 5(a), 6 and 7 of Ref. 20, Figure 3 of Ref. 21, and Figures 1 and 2 of Ref. 22) and other C-T materials<sup>24</sup>. Similar patterns appear also in the well known ferroelectric BaTiO<sub>3</sub>, specifically Figures 2(a) and 8(b) of Ref. 2; they should appear in other elastic/electric and elastic/magnetic ferroics provided that the elastic energy dominates the electric and magnetic energies, as it does<sup>2</sup> in BaTiO<sub>3</sub>. Banded structures were found also in a phase-field study<sup>14</sup>.

All three variants appear in Figure 1, but not equivalently. The structures consist of two primary bands, here red and green; the width of the primaries is determined by the system size in Figure 1 and, one assumes, by the grain size in experiment. Each primary is penetrated by the third variant, here blue; neither primary contains domains of the other. Within each primary, the host and the third variant form secondary bands; the ratio of the width of the host variant to the width of the third variant in the secondary bands is ideally 2:1 so that the three variants appear with equal volume fractions<sup>20,26</sup>. The same ratio was found in Refs. 2, 25, which found also the optimal value of the period of the primary bands to that of the secondary bands.

Figure 1(a) shows a fully converged<sup>31</sup> structure; it has the lowest energy of seven states found in 24 quenches with the same parameters. The front face shows chevron (or herringbone) structures; the blue domains are continuous across the red-green boundaries, where they bend through 90° and are slightly distorted as well.

Figure 1(b) shows another fully converged structure obtained with the same parameters as part (a); it has a higher energy (the third lowest of the seven states) and so is metastable. Some of the blue variants form chevrons, as in part (a), but some terminate at the red-green boundaries; the walls occasionally deviate from the 110 planes. Presumably the higher energy relative to part (a) results in part from the terminations and the

deviations; both are seen experimentally, for example in Figures 4(a), 5(a) and 6 of Ref. 20.

Figure 1(c), for a 256<sup>3</sup> system with stiffer parameters, shows a quasi-static<sup>31</sup> configuration with a mixture of continuing and terminating variants. The system is large enough to show the secondary banding clearly, but it is too small and has too many imperfections to display well the 2:1 ratio discussed above. Of the two other simulations performed with the same parameters, one gave no terminations and not surprisingly a lower energy, and the third gave more terminations and a larger energy.

In addition to these banded structures, we found lamellar structures in smaller systems (64<sup>3</sup>), particularly for stiffer parameters; the agreement with the lamellar  $\leftrightarrow$  banded transition analysed in Ref. 2, 25 is however largely illusory, for the order parameters cannot approach their optimal values due to the length constraint in the third direction. We found also intermediate structures in which the narrow variant appears in only one of the two primary bands. Finally, a few systems gave very different tweed-like or basket-weave structures, of all three variants, that seem not to be observed in experiment.

### B. Transient structures

In all our late-time banded structures (not just those of Figure 1), walls collide only at boundaries between the primary bands. Within each primary red (green) band, (a) the red-blue (green-blue) walls adopt only one of the two possible orthogonal orientations<sup>16</sup>, and (b) the other primary, the green (red) variant, is absent.

Walls colliding within the primary bands are however observed; examples are the  $A_3$  band in Figure 6 of Ref. 20, Figure 7(b) of Ref. 20, Figure 3 of Ref. 21, and Figure 11 of Ref. 22. Because we obtain only two primary bands, neither did we observe the  $A_2$  and  $A_4$  bands in Figure 6 of Ref. 20; these contain the same two variants as the  $A_1$  band but with the orthogonal wall orientation.

Perhaps our systems are too small to show these effects, perhaps the experimental systems are incompletely relaxed; that different experimental conditions can give different patterns<sup>2</sup> may be relevant here. We have however found some of these features in transient structures of a 256<sup>3</sup> system; 128<sup>3</sup> systems are too small to show interesting features clearly.

The important aspects of Figures 2(a) and (b) are the following.

1. Needle twins: The top face of part (a) shows a band of green needle twins in the red primary band, and also a band of blue needle twins in the green primary band; needles appear also elsewhere. In part (b), some needles have advanced and some have retracted. Needle twins are found for example in leucite (Figure 3 of Ref. 23).
2. Collisions of identical variants: In the green primary band on the top face, green/blue walls collide with green/blue walls of the other orientation, forming modu-

lated structures. Figure 11 of Ref. 22 shows a similar pattern in zirconia, “a rather exceptional case”, also formed by orthogonal colliding walls. As in Refs. 8, 9, we ascribe these modulations, and also the structures in Figure 3(b) of Ref. 23, to formation of wedge disclinations between two identical but differently rotated variants; the same explanation applies to tip splitting, in some cases.

3. A split tip: Tip splitting seems to occur only rarely in C-T materials (relative to T-O materials), presumably because of the extra freedom afforded by three variants; an example is Figure 3 of Ref. 23. We found only one split tip, an indistinct one at that, at the right side of the top face in part (a); this is of course a transient configuration. Split tips appear in the statics of some simulations<sup>8,14</sup>, but only at the interface with parent material; they are more frequent in transient structures<sup>9</sup>.

4. Collisions of different variants: In the top faces of both parts (a) and (b), green needle twins collide orthogonally with, or come near, blue variants; collisions occur also in the lower front face of part (a). No special features result from the collisions, which have not been noted in any experiment known to us.

Figure 2(c) shows the same system at the later time  $t = 30$ . Many of the defects in part (b) have disappeared in this quasi-static wall configuration; the walls are straighter, but in this relatively soft system they still bend where the third variant (here blue) terminates.

Inspection of the dilatational and shear strains of late-time structures shows, not surprisingly, that their magnitude is maximum in the wall-collision regions. We investigated also the early stages of growth initiated by locally perturbing the parent phase at a temperature well below  $T_c$ ; the growth occurs predominantly along spikes in the 111 directions and planes in 110 directions, producing a noncompact object.

## ACKNOWLEDGMENTS

Some of the numerical simulations were performed at the Computation and Visualisation Centre at Memorial University of Newfoundland. We are grateful to E. H. Kisi for pointing out the similarity of our patterns to those observed in zirconia and for informing us of Refs. 20–22 and 26, to J. Kreisel for informing us of Ref. 27, to T. Hahn for informing us of Ref. 2, to M. Hayakawa for discussions, and to NSERC of Canada for financial support.

## APPENDIX A

We solved Eqs.(24) using periodic boundary conditions on the displacement  $\mathbf{u}$ . Since only qualitative comparison with experiment seems possible at present, and because we wished to obtain results qualitatively applicable to many C-T materials, we scaled the energy, the

strains and the length; this scaling requires neglect of the nonlinear term in the strain tensor  $\eta$ . We chose the values  $B_2 = 3 \times 10^3$  and  $C_2 = 2 \times 10^6$  so that the transition occurs at  $A_2 = 1$ , and the scaled strain at  $T_c$  is  $e_{30}(T_c) = 10^{-3}$ , an arbitrary value. We chose  $D_2 = 1$  to set the scale for the domain-wall width<sup>18</sup>. The number of parameters in the free-energy density is then reduced from six to three, the scaled stiffnesses  $A_1$  and  $A_4$  and the scaled  $T$ -like variable  $A_2$ . Results for other parameter values are easily obtained by scaling back to the original variables.

The viscosity coefficients  $A'_j$  appearing in Eq. (24) are not known from microscopic theory. Neither we expect can they be determined from experiments such as ultrasonic attenuation that operate on time scales very different from those governing domain-wall motion (as distinct from the “twin cry” in some materials). Lacking experiments that might determine the relevant coefficients, we chose the unit of time so that  $A'_2 = 1$ ; lacking a reason to do otherwise, we chose  $A'_1 = A'_4 = 1$  also.

Each time step began with the Fourier coefficients  $\tilde{u}_j(\mathbf{k}, t)$  at time  $t$ . The left-hand sides of Eqs. (24) are linear in the strains and so the space derivatives are obtained by multiplication in Fourier space; our approximations for the derivatives are described below. The linear terms on the right-hand sides are found in the same way. To obtain the nonlinear terms  $R_i^{NL}$  in Fourier space, we formed the Fourier coefficients of the strains  $e_2$  and  $e_3$ , transformed them to find the strains in real space, found the nonlinear terms  $\mathcal{G}_2^{NL}$  and  $\mathcal{G}_3^{NL}$  by multiplication (replacing the strains point by point), transformed the two terms back to Fourier space, and multiplied to obtain the space derivatives in Fourier space. The solutions were advanced in time by an Euler step (usually  $\Delta t = 4 \times 10^{-3}$ ); solution of three linear algebraic equations then gives the three components  $\tilde{u}_j(\mathbf{k}, t + \Delta t)$  in Fourier space. To monitor the convergence, we found the energy, the root-mean-square order-parameter strains and right-hand sides of Eq.(24), etc, every 10 or 20 time steps.

The above computational scheme requires storage of five matrices, three for the  $\tilde{u}_j(\mathbf{k}, t)$  and two for the strains  $e_2$  and  $e_3$  (or  $\mathcal{G}_2^{NL}$  and  $\mathcal{G}_3^{NL}$ ). The fast Fourier transforms were performed using the Numerical Recipes routine `fourn`<sup>33</sup>, which deals with complex matrices. The full executable file for a  $256^3$  system requires 1.35GB of storage. Savings of about two in storage and execution time would be obtained by use of routines for real matrices, although some expense in coding and clarity. We have also obtained static structures by conjugate-gradient minimization of the energy<sup>33</sup>. The latter method is preferable in some respects to solving the equations of motion, and we have used it to verify the correctness of some of our  $64^3$  and  $128^3$  results; it requires however roughly 7 times more storage, well in excess of that available to us for  $256^3$  systems.

The first and second derivatives were obtained from obvious generalizations of the 1d finite-difference approximations

$$\frac{df(0)}{dx} \approx \frac{2}{3h} \left\{ [f(h) - f(-h)] - \frac{1}{8} [f(2h) - f(-2h)] \right\} \quad (\text{A1})$$

$$\frac{d^2f(0)}{dx^2} \approx \frac{4}{3h^2} \left\{ [f(h) + f(-h) - 2f(0)] - \frac{1}{16} [f(2h) + f(-2h) - 2f(0)] \right\} \quad (\text{A2})$$

If the Fourier coefficients are defined by

$$f(\mathbf{r}) = \sum_{jkl} a_{jkl} e^{2\pi i(jx+ky+lz)/L} \quad (\text{A3})$$

with period  $L = Nh$  in each variable, then the first and second derivatives are approximated by

$$\frac{\partial}{\partial x} \rightarrow \frac{i}{3h} \sin(2\pi jh/L) [3 + 2 \sin^2(\pi jh/L)] \quad (\text{A4})$$

$$\frac{\partial^2}{\partial x^2} \rightarrow \frac{-4}{3h^2} \sin^2(\pi jh/L) [3 + \sin^2(\pi jh/L)] \quad (\text{A5})$$

in Fourier space. In obtaining second-derivative terms like  $\partial_1^2$  in Eq.(24), it is important to use Eq.(A5) rather than Eq.(A4) twice, for the latter vanishes at  $j = N/2$ .

The space step size  $h$  must be chosen as a reasonable compromise between the conflicting demands of large physical size  $L = Nh$  on the one hand and accuracy on the other. Our values  $h = 0.5$  at  $A_2 = -2$  and  $h = 0.25$  at  $A_2 = -20$  were established as follows.

We first performed 48 quenches at  $A_2 = -20$  with  $A_1 = A_4 = 100$  on systems of identical linear size  $L = Nh$ ; 24 of these quenches used  $(N, h) = (128, 0.125)$  and 24 used  $(N, h) = (64, 0.25)$ . The larger step size gave 4 states, each of which was clearly identified with a state found for the smaller  $h$ . The energies of the 4 states common to the two sets of quenches agreed to better than 1 part in 2000 (relative to the uniform product phase) and the relative frequencies of occurrence were comparable. The smaller step size gave however 3 additional states, each once. Since  $h = 0.25$  is satisfactory at  $A_2 = -20$  and since the variational wall width<sup>18</sup> scales as  $1/e_{30}$ , one expects  $h = 0.5$  to be satisfactory at  $A_2 = -2$  where  $e_{30}$  is half the value at  $A_2 = -20$ . Less extensive tests carried out at  $A_2 = -2$  with  $A_1 = A_4 = 100$  gave comparable results for  $(N, h) = (128, 0.25)$  as against  $(64, 0.5)$ . Similar tests with  $A_1 = A_4 = 1000$  at both values of  $A_2$  gave the same conclusions.

In passing, we remark that the number of metastable states found in the quenches of the previous paragraph and in the quenches used for parts (a) and (b) of Figure 1 is smaller than found in a T-O study<sup>8</sup> of clamped systems of comparable linear size; the difference is due to the different boundary conditions.

FIG. 1. Late-time domain patterns. The faces of each display cube are cubic 100 planes; the red, green and blue regions correspond to the three tetragonal variants; the domain walls (black) lie optimally in cubic 110 planes. Parts (a) and (b) show fully converged<sup>31</sup> patterns (both at  $t \approx 70$ ) obtained in  $128^3$  systems using different starting configurations but otherwise identical parameters ( $A_1 = A_4 = 100$ ); pattern (b) is a metastable state with higher energy than pattern (a). Part (c) shows a quasi-static<sup>31</sup> configuration in a  $256^3$  system at  $t = 140$  with stiffer parameters ( $A_1 = A_4 = 500$ ). The temperature parameter is  $A_2 = -20$  for all three parts.

FIG. 2. Snapshots of a  $256^3$  system as it relaxes from random initial displacements. The faces are cubic 100 planes. The temperature parameter is  $A_2 = -20$  and the stiffnesses are  $A_1 = A_4 = 100$ . Parts (a) and (b) are transient structures at times  $t = 2.2$  and  $3.6$  respectively; part (c) is a quasi-static pattern at  $t = 30$ .

\* Electronic address: jacobs@physics.utoronto.ca

† Electronic address: curnoe@physics.mun.ca

‡ Electronic address: desai@physics.utoronto.ca

<sup>1</sup> K. Aizu, J. Phys. Soc. Jpn. **27**, 387 (1969).

<sup>2</sup> G. Arlt, J. Materials Science **25**, 1655 (1990).

<sup>3</sup> E. K. H. Salje, *Phase Transitions in Ferroelastic and Coelastic Crystals*, Cambridge University Press (1993).

<sup>4</sup> Y. Ma, E. H. Kisi and S. J. Kennedy, J. Am. Ceram. Soc. **84**, 399 (2001).

<sup>5</sup> G. R. Barsch and J. A. Krumhansl, Phys. Rev. Lett. **53**, 1069 (1984).

<sup>6</sup> A. E. Jacobs, Phys. Rev B **31**, 5984 (1985).

<sup>7</sup> S. H. Curnoe and A. E. Jacobs, Phys. Rev. B **63**, 094110 (2001).

<sup>8</sup> A. E. Jacobs, Phys. Rev. B **61**, 6587 (2000).

<sup>9</sup> S. H. Curnoe and A. E. Jacobs, Phys. Rev. B **64**, 064101 (2001).

<sup>10</sup> T. Lookman, S. R. Shenoy, K. Ø. Rasmussen, A. Saxena, and A. R. Bishop, Phys. Rev. B **67**, 024114 (2003).

<sup>11</sup> A. G. Khachatryan and G. A. Shatalov, Sov. Phys. JETP **29**, 557 (1967); A. G. Khachatryan, Fiz. Tverd. Tela **8**, 2170 (1966) [English translation: Soviet Physics - Solid State **9**, 2163 (1967)]; A. G. Khachatryan, *Theory of Structural Transformations in Solids*, John Wiley and Sons, New York, 1983.

<sup>12</sup> Y. H. Wen, Y. Wang, and L. Q. Chen, Acta Mater. **47**, 4375 (1999); Y. H. Wen, Y. Z. Wang, and L. Q. Chen, Philos. Mag. **A80**, 1967 (2000).

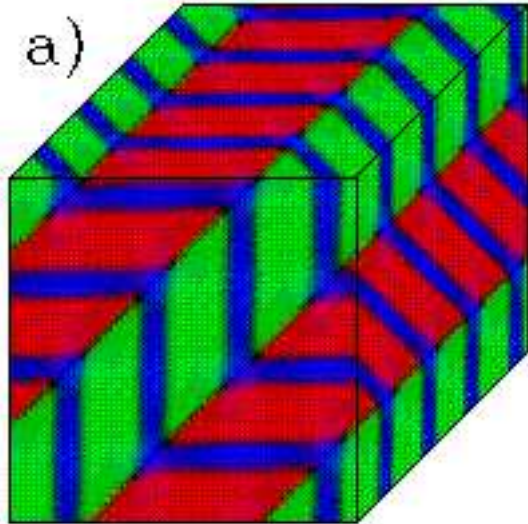
<sup>13</sup> Y. Wang and A. G. Khachatryan, Acta Mater. **45**, 759 (1997);

<sup>14</sup> A. Artemev, Y. Jin, and A. G. Khachatryan, Acta Mater. **49**, 1165 (2001).

<sup>15</sup> S. Kartha, J. A. Krumhansl, J. P. Sethna, and L. K. Wickham, Phys. Rev. B **52**, 803 (1995).

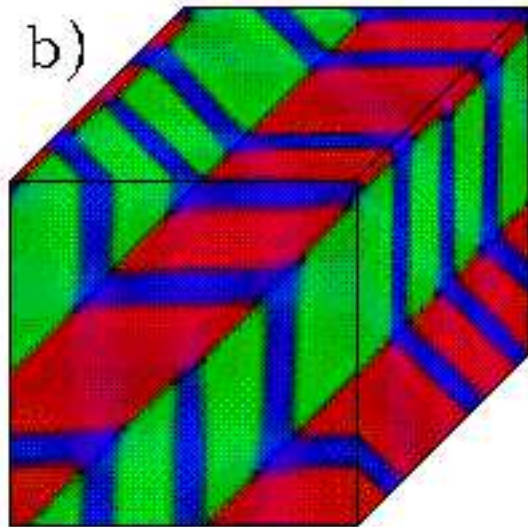
- <sup>16</sup> J. Sapriel, Phys. Rev. B **12**, 5128 (1975).
- <sup>17</sup> G. R. Barsch and J. A. Krumhansl, Proceedings of the International Conference on Martensitic Transformations (1992), page 53, Monterey Institute for Advanced Studies (Monterey, 1993).
- <sup>18</sup> S. H. Curnoe and A. E. Jacobs, Phys. Rev. B **62**, R11925 (2000).
- <sup>19</sup> N. A. Pertsev, J. Novak, and E. K. H. Salje, Philos. Mag. A **80**, 2201 (2000).
- <sup>20</sup> M. Hayakawa, M. Tada, H. Okamoto, and M. Oka, Trans. Japan Institute of Metals **27**, 750 (1986). In this and other articles<sup>21,22,4</sup> on zirconia, the tetragonal phase is stabilized by the addition of 2 or 3 mol % yttria. The foil orientation for Figure 4(a) is (0 $\bar{2}$ 1) whereas our Figure 1 shows cubic 100 faces.
- <sup>21</sup> M. Hayakawa, N. Kuntani, and M. Oka, Materials Science Forum **56-58**, 363 (1990): Proceedings of the International Conference on Martensitic Transformations (1989).
- <sup>22</sup> D. Baither, B. Baufeld, U. Messerschmidt, A. H. Foitzik, and M. Rühle, J. Am. Ceram. Soc. **80**, 1691 (1997).
- <sup>23</sup> D. C. Palmer, A. Putnis, and E. K. H. Salje, Phys. Chem. Minerals **16**, 298 (1988).
- <sup>24</sup> Reference 20 cites articles reporting similar structures in the C-T ferroelastic alloys In-Tl, Fe-Pd and Mn-Cu.
- <sup>25</sup> N. A. Pertsev and G. Arlt, Ferroelectrics **132**, 27 (1992).
- <sup>26</sup> M. Hayakawa and M. Oka, Materials Science Forum **56-58**, 383 (1990).
- <sup>27</sup> M. Geday, J. Kreisel, A. M. Glazer, and K. Roleder, J. Appl. Cryst. **33**, 909 (2000).
- <sup>28</sup> P. Klouček and M. Luskin, Continuum Mech. Thermodyn. **6**, 209 (1994); Math. Comput. Modell. **20**, 101 (1994).
- <sup>29</sup> K. Ø. Rasmussen, T. Lookman, A. Saxena, A. R. Bishop, R. C. Albers, and S. R. Shenoy, Phys. Rev. Lett. **87**, 055704 (2001).
- <sup>30</sup> S. R. Shenoy, T. Lookman, A. Saxena, and A. R. Bishop, Phys. Rev. B **60**, R12537 (1999).
- <sup>31</sup> Fully converged means that numerical errors prevented further change in the energy, root-mean-square strains, etc. Quasi-static means that gross features of the pattern are fixed; further relaxation occurs, without wall annihilation or creation, through wall migration so as to align where possible identical variants across boundaries. The relaxation times for this process are very large and increase rapidly with the system size and.
- <sup>32</sup> Whether the narrow domains in the banded structures were red, green or blue depended on the initial conditions. In preparing the Figures, we used where necessary symmetry operations to make the narrow domains blue.
- <sup>33</sup> W. H. Press, S. A. Teukolsky, W. T. Vetterling, and B. P. Flannery, Numerical Recipes in FORTRAN: The Art of Scientific Computing (Cambridge University Press, 1992).

a)

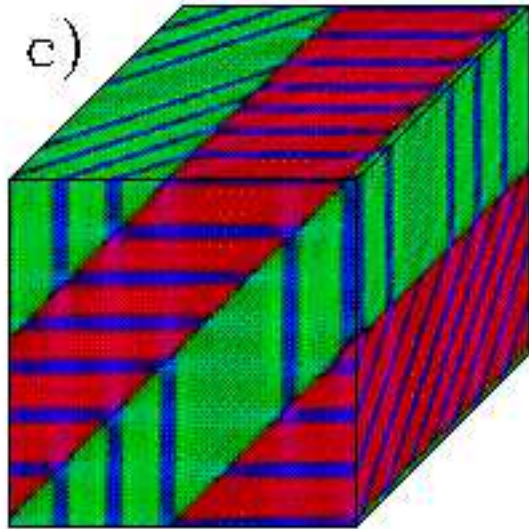




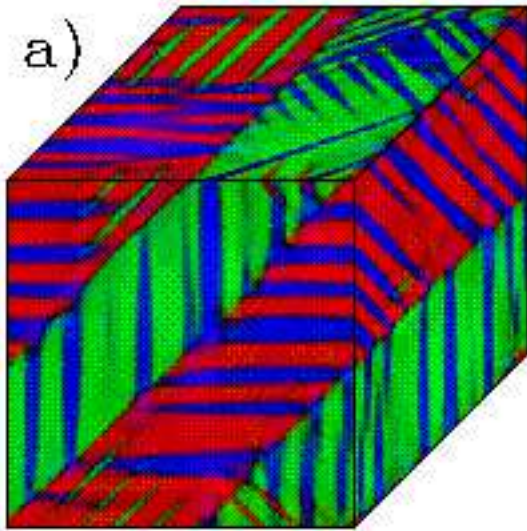
b)



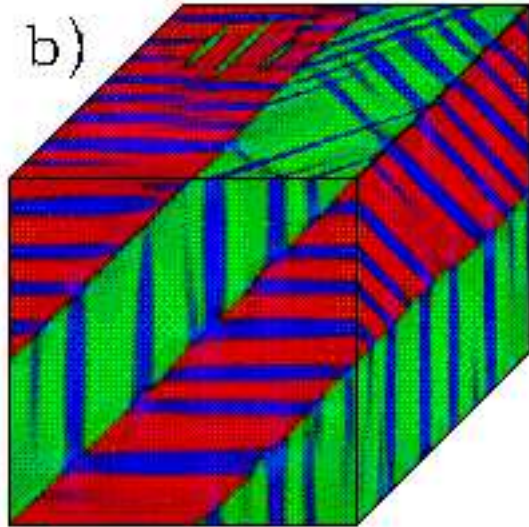
c)



a)



b)



c)

